

Tuning transport in solid-state Bose-Fermi mixtures by Feshbach resonances

Caterina Zerba,^{1, 2, *} Clemens Kuhlenkamp,^{3, 1, 2, *} Léo Mangeolle,^{1, 2, *} and Michael Knap^{1, 2}

¹Technical University of Munich, TUM School of Natural Sciences, Physics Department, 85748 Garching, Germany

²Munich Center for Quantum Science and Technology (MCQST), Schellingstr. 4, 80799 München, Germany

³Department of Physics, Harvard University, Cambridge, Massachusetts 02138, USA

(Dated: June 17, 2025)

Transition metal dichalcogenide (TMD) heterostructures have emerged as promising platforms for realizing tunable Bose-Fermi mixtures. Their constituents are fermionic charge carriers resonantly coupled to long-lived bosonic interlayer excitons, allowing them to form trion bound states. Such platforms promise to achieve comparable densities of fermions and bosons at low relative temperatures. Here, we predict the transport properties of correlated Bose-Fermi mixtures close to a narrow solid-state Feshbach resonance. When driving a hole current, the response of doped holes, excitons, and trions are significantly modified by the resonant interactions, leading to deviations from the typical Drude behavior and to a sign change of the exciton drag. Our results on the temperature-dependent resistivities demonstrate that near resonance interaction effects dominate over established conventional scattering mechanisms in these solid-state Bose-Fermi mixtures.

Unconventional phases in solids are predicted to arise when a Fermi surface is strongly coupled to bosonic excitations, such as phonons, spin- and density-wave fluctuations, and collective modes emerging in the vicinity of phase transitions [1–8]. However, isolating relevant interaction channels is challenging, as electrons are typically coupled simultaneously to multiple bosonic modes. This motivates the exploration of Bose-Fermi mixtures in more controlled settings of transition-metal-dichalcogenide (TMD) heterostructures [9–18]; complementary regimes are accessible in ultracold atomic gases as well [19–24]. TMDs offer the advantage that low relative temperatures are reachable [15]. In these settings, fermions are introduced by charge doping and high densities of long-lived bosons are realized as tightly-bound interlayer excitons [25]. Excitons interact with doped charges [10, 26–28] forming fermionic bound states, referred to as trions, which have been observed to remain stable even at finite densities [15, 16]. While theoretical studies have shown that low temperature Bose-Fermi mixtures in TMDs could host sought-after unconventional phases [29–32], surprisingly many properties of such mixtures at intermediate temperatures remain unexplored. Recent experimental advances [33, 34] are furthermore enabling new theoretical and experimental avenues for studying correlated Bose-Fermi mixtures through transport; an approach that is very challenging in cold atom setups.

In this work, we theoretically investigate transport properties of tunable solid-state Bose-Fermi mixtures in TMD heterostructures near a Feshbach resonance. In this regime, we map the strongly-interacting hole-exciton problem into an effective, analytically tractable theory that includes all three particle species: holes, excitons and trions. Our analysis shows how strongly interacting Bose-Fermi mixtures can be investigated in the vicinity of a solid-state Feshbach resonance. We uncover a rich phenomenology by considering a selectively driven hole

current and tuning the exciton-hole scattering into resonance. Our results show that the conductivities of all three particle species depend sensitively on one external parameter, the perpendicular electric field, which tunes the relative energy of the trion. Remarkably, this exciton-hole scattering effect dominates the transport properties below the phonon temperature scale, and induces a sign-changing exciton drag conductivity in a broad parameter regime. As another striking effect we find that the resistivity of the system exhibits a strong, non-monotonic temperature dependence, as well as an unconventional ac response beyond Drude phenomenology.

Model.— Inspired by recent experiments [10, 15, 16], we propose a setting composed of three monolayer TMDs, where the top layer is hole-doped and separated from the other layers by hexagonal boron nitride (hBN) of thickness d , see Fig. 1 (a). The relative energy of charges in the middle layer is tuned by a perpendicular electric field E_z . This imposes an electrostatic potential difference eE_zd , where e is the elementary charge. We consider fields E_z that suppress tunneling of unbound holes to the middle layer, see Fig. 1 (a,b). The perpendicular electric field and the density of doped charges are fixed independently by tuning the voltage of the top and middle layers, as shown in Ref. [10]. Interlayer excitons between the middle and the lower layer are optically or electrically injected, and the applied voltage does not relevantly affect their density since they are tightly bound [10, 35]. Interlayer excitons are selectively excited, as their binding energy is in general different from that of other excitations, e.g. intralayer excitons. Due to the small overlap of the hole and electron wavefunctions, their lifetime can exceed hundreds of ns, which allows us to treat excitons as well-defined bosonic particles [25].

The Bose-Fermi mixture of excitons and holes is strongly interacting, which is reflected by the existence of a trion bound state. Scattering is tuned in resonance by changing the field E_z . It is possible to approx-

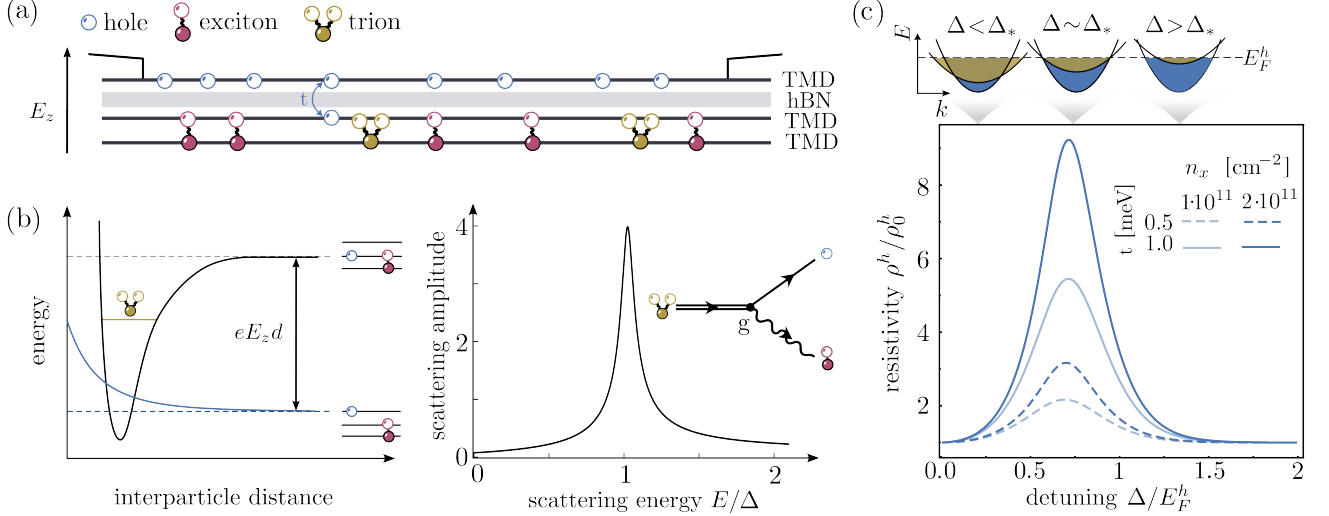


FIG. 1. Setup, particle-like trion bound state and enhanced transport close to resonance. **a)** Proposed trilayer TMD structure. The system realizes a Bose-Fermi mixture with doped charges (holes) in the upper layer and strongly bound interlayer excitons in the lower two layers. A longitudinal electric field is applied only to the top layer via direct contacts that drive a hole current. **b)** Solid-state Feshbach resonance. Left: The energy of a spatially separated exciton-hole pair (blue curve) can be tuned close to the energy of the trion (yellow) by the perpendicular electric field, which shifts the energy of the trion to $E_t^0 + \Delta = eE_z d$. Right: The exciton-hole scattering amplitude $|f(E)|$ (see supplemental material [36]) is resonantly enhanced around the shifted trion energy due to the narrow Feshbach resonance. **c)** Resistivity of holes in the upper layer ρ^h as a function of the detuning Δ , calculated at $T = 5.8$ K. The resistivity is strongly enhanced close to the resonance condition $\Delta \sim \Delta_*$, where the hole and trion Fermi surfaces have the same size. Top: Sketches to illustrate the hole and trion Fermi seas as a function of Δ .

imate multiple (resummed) scattering events between holes and excitons as an interaction mediated by the trion. This approximation, which is accurate near the Feshbach resonance, is discussed further in the Supplemental Material [36], and makes the transport problem analytically tractable. The bare hole-exciton-trion vertex g gives the effective interaction between these three species, and is represented in Fig. 1 (b). Starting from the microscopic exciton-hole Hamiltonian, we identify $g \simeq \left(\frac{2\pi}{m_{\text{red}}|E_t^0|}\right)^{1/2} t$, where t is the hole coherent tunneling rate, E_t^0 the trion binding energy, $m_{\text{red}}^{-1} = m_h^{-1} + m_x^{-1} = (3/2)m_h^{-1}$, and we have assumed that g is momentum-independent [20, 28, 29]. For $eE_z d \geq E_t^0$, the trion decays into an exciton-hole pair at a rate proportional to t^2 , which can be much smaller than the relevant Fermi energies [10]. This allows us to treat triions as sharp quasi-particles whose energy is tuned by the Feshbach resonance, see Fig. 1 (b). Even for finite hole and exciton densities, the trion retains a quasi-particle peak, provided $g \ll E_F^h/\sqrt{n_x}$, which we use as a perturbative parameter.

The resulting system is well described by holes, excitons and triions with quadratic dispersions $\epsilon_{h,\mathbf{p}} = \frac{\mathbf{p}^2}{2m_h} - \mu_h$, $\omega_{\mathbf{k}} = \frac{\mathbf{k}^2}{2m_x} - \mu_x$ and $\epsilon_{t,\mathbf{p}} = \frac{\mathbf{p}^2}{2m_t} - \mu_t + \Delta$, respectively, where $\Delta = eE_z d - E_t^0$. The trion mass is $m_t = m_x + m_h$. We assume the system has reached

thermal equilibrium, which fixes the chemical potentials to satisfy $\mu_h + \mu_x = \mu_t$ [37]. The effective Hamiltonian describing the solid-state Bose-Fermi mixture is then

$$\hat{H} = \int \frac{d^2 \mathbf{p}}{(2\pi)^2} (\epsilon_{h,\mathbf{p}} \hat{c}_{\mathbf{p}}^\dagger \hat{c}_{\mathbf{p}} + \epsilon_{t,\mathbf{p}} \hat{m}_{\mathbf{p}}^\dagger \hat{m}_{\mathbf{p}}) + \int \frac{d^2 \mathbf{k}}{(2\pi)^2} \omega_{\mathbf{k}} \hat{x}_{\mathbf{k}}^\dagger \hat{x}_{\mathbf{k}} + g \int \frac{d^2 \mathbf{p}}{(2\pi)^2} \frac{d^2 \mathbf{k}}{(2\pi)^2} (\hat{m}_{\mathbf{p}+\mathbf{k}}^\dagger \hat{c}_{\mathbf{p}} \hat{x}_{\mathbf{k}} + \text{h.c.}), \quad (1)$$

where \hat{c}^\dagger , \hat{x}^\dagger and \hat{m}^\dagger (\hat{c} , \hat{x} and \hat{m}) are the hole, exciton and trion creation (annihilation) operators.

Unless stated otherwise, we will use the following parameters: hole Fermi energy $E_F^h = 5$ meV, $E_t^0 = -10$ meV, $t = 1$ meV, $n_x = 2 \cdot 10^{11} \text{ cm}^{-2}$ and $m_h = 0.5 m_e$ with m_e the free electron mass, and set $\hbar = 1$ [10, 15, 16, 38, 39]. Throughout the work we model extrinsic sources of momentum relaxation (e.g. disorder) for all species by a momentum-independent relaxation time $\tau_0 = 10$ ps, motivated by recent transport experiments [33, 34, 40]. The extrinsic sources of relaxation may include other excitations and few-body complexes, which are off-resonant and whose effect thus varies slowly with E_z in the regime of interest. We emphasize that our results do not depend qualitatively on the chosen parameters.

Methods.— Electrical contacts are placed such that a longitudinal electric field is applied only to the charge-doped layer, as shown in Fig. 1(a). This induces a charge

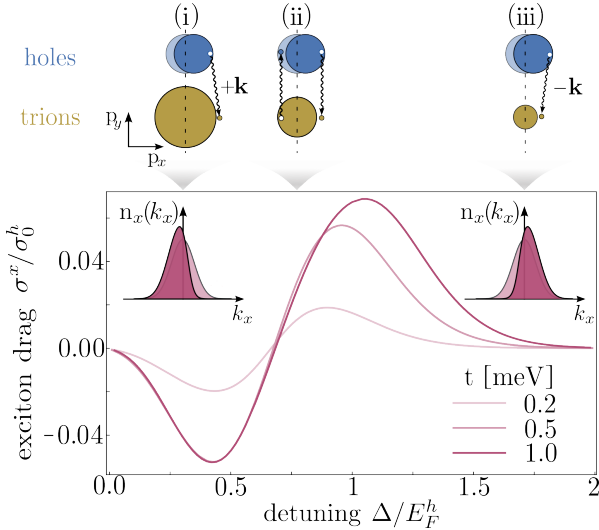


FIG. 2. Sign-changing exciton drag. Exciton drag conductivity as a function of detuning Δ evaluated at temperature $T = 5.8$ K. The backflow of excitons, $\sigma^x < 0$, for small detuning can be understood from the interplay of energy and momentum conservation and Pauli exclusion. Upper panels: Sketches of the relevant scattering processes for exciton drag. (i) A hole (from the blue Fermi sea) absorbs a right-moving exciton (squiggly arrow) to form a trion (above the yellow Fermi sea). This depletes right-moving excitons and skews the exciton distribution $n_x(k_x)$ (red) against the direction of the hole current. (ii) Close to resonance, scattering processes primarily involve small-momentum excitons, leading to a small exciton drag. (iii) A hole absorbs a left-moving exciton, which skews the exciton distribution $n_x(k_x)$ in the direction of the hole current.

current $j_a^h = \sigma_{ab}^h E_b$ in the upper layer, where σ_{ab}^h is the hole conductivity tensor and $a, b \in \{x, y\}$ are the longitudinal and transverse directions. Since we are considering linear response in an isotropic and time-reversal symmetric model, $\sigma_{ab}^h = \delta_{ab}/\rho^h$ with ρ^h the hole resistivity. Excitons and trions do not couple to the electric field directly. Instead, their particle currents, J_a^x and J_a^t , induced in the middle and lower layers, arise purely from drag effects mediated by the hole current via many-body scattering. We define the corresponding conductivity as $\sigma_{ab}^i = e J_a^i / E_b$ for $i \in \{x, t\}$. We analyze the currents induced in the system for all three species of particles, as a function of detuning Δ and temperature T . Using a kinetic theory, where the collision integrals are obtained from a perturbative calculation of the self-energies [41], we derive and solve a set of three coupled Boltzmann's equations for the particle distributions. A perturbative calculation of the hole conductivity based on Kubo's formula [42] yields similar results, up to quantitative corrections in the vicinity of the resonance. Further details about both methods, and a comparison, are reported in the Supplemental Material [36].

Tunable hole transport.— In our system, holes

exhibit a tunable resistivity ρ^h : the resistivity ρ^h is governed not only by the intrinsic background scattering rate τ_0^{-1} that sets the constant background resistivity $\rho_0^h = 2\pi/(\mu_h e^2 \tau_0) = 1/\sigma_0^h$, but crucially also by many-body interactions with the bosonic interlayer excitons that depend on the perpendicular electric field $E_z = (\Delta + E_t^0)/ed$. By solving the coupled transport equations, we find that the resistivity ρ^h exhibits a strong resonant behaviour as a function of the detuning Δ , as demonstrated in Fig. 1(c) for different tunneling rates t and exciton densities n_x . The tunability of the resistivity originates from exciton-hole scattering, as the perpendicular electric field E_z sweeps through the Feshbach resonance and sets the size of the trion Fermi surface. For small Δ the trion Fermi surface is large, and shrinks for larger values of Δ until it eventually vanishes for $\Delta \gtrsim \mu_h$. The contribution of interactions to the hole resistivity is determined by the hole many-body scattering rate, which to order $O(g^2)$ reads

$$\text{Im}\Sigma_h^R(\mathbf{p}, \epsilon_h, \mathbf{p}) = |g|^2 \int \frac{d^2\mathbf{k}}{(2\pi)^2} (n_F(\epsilon_{t, \mathbf{p}+\mathbf{k}}) + n_B(\omega_{\mathbf{k}})) \times 2\pi \delta(\omega_{\mathbf{k}} + \epsilon_h, \mathbf{p} - \epsilon_{t, \mathbf{p}+\mathbf{k}}), \quad (2)$$

with n_B and n_F the Bose and Fermi distributions. The conservation of energy in Eq. (2) ensures that the trion energy matches the combined energies of the exciton and hole. This captures the dominant contribution of the resonant peak to the scattering amplitude shown in Fig. 1(b), and reflects the existence of a metastable Feshbach molecule.

At low temperatures, Eq. (2) is dominated by processes involving small exciton momentum \mathbf{k} , where the bosonic population $n_B(\omega_{\mathbf{k}})$ is largest. Many-body scattering is then maximized when the energy of a trion is resonant with the energy of a hole nearby the Fermi surface. In our model this takes place when the two Fermi surfaces are of the same size, which occurs when Δ is tuned to

$$\Delta_{\star} = (1 - m_h/m_t) \mu_h = (2/3) \mu_h. \quad (3)$$

We find that tuning the electric field on resonance strongly enhances the hole resistivity by about an order of magnitude, see Fig. 1(c). The background Drude resistivity ρ_0^h is recovered in the limit $\Delta \leq 0$, where the phase space volume satisfying the constraint in Eq. (2) vanishes, and for sufficiently strong detuning $\Delta \gg 1$ as scattering becomes off-resonant.

Interaction induced drag transport.— Although excitons are charge neutral and spatially decoupled from the driven layer, they experience drag effects due to exciton-hole scattering. The resulting drag conductivity σ^x can be experimentally measured by separately contacting the lower two layers. Because it is entirely interaction-driven, the exciton conductivity is highly tunable with the electric field. Three distinct regimes are identified (Fig. 2):

(i) For $\Delta < \Delta_*$, the hole Fermi surface is smaller than the trion Fermi surface. Thus holes driven out of equilibrium with $p_x > 0$ combine mainly with excitons carrying positive momenta $k_x > 0$, depleting the exciton distribution for $k_x > 0$. This results in an exciton current $J_x^x < 0$ that flows in the opposite direction to the hole current.

(ii) For $\Delta \simeq \Delta_*$, the exciton drag σ^x vanishes and changes sign. Dominant scattering results from excitons with small momenta, which carry negligible current. This is in stark contrast with the hole resistivity for which many-body scattering is most dominant in this regime.

(iii) For $\Delta > \Delta_*$, the trion Fermi surface is smaller than the hole Fermi surface. Thus holes with $p_x > 0$ dominantly combine with excitons with $k_x < 0$, depleting the exciton distribution for $k_x < 0$, which yields an exciton current $J_x^x > 0$ flowing in the direction of the hole current.

The exciton drag increases with the hybridization t , see Fig. 2. Since excitons are charge neutral, their conductivity scales to leading order as $\sigma^x \sim g^2/\rho^h$. Away from resonance and for small tunneling rates $t \ll 1/\tau_0$ the hole resistivity remains close to its background value $\rho^h \approx \rho_0^h + O(g^2)$. Consequently, the exciton conductivity follows $\sigma^x \sim g^2/\rho_0 \sim t^2/\rho_0$, as $g \sim t$. Near resonance, however, the hole resistivity is governed by many-body scattering, which also scales as $\rho^h \sim t^2$. This implies a saturation of σ^x with increasing tunneling t , see Fig. 2. This intuitive picture, which focuses on the thermally dominant scattering processes, is confirmed by our calculations, which systematically include all such scattering processes, as detailed in the Supplemental Material [36]. Our mechanism should be distinguished from exciton drag resulting from polaron formation in monolayer settings [43]. The exciton flow could be accessed experimentally by measuring the charge currents in the bottom ($j_B = -\sigma^t E - \sigma^x E$) and middle ($j_M = 2\sigma^t E + \sigma^x E$) layers separately, allowing to extract $\sigma^x = -(2j_B + j_M)/E$.

Non-monotonous temperature dependence.— Conventional scattering due to disorder and phonons typically leads to an electronic resistivity monotonically increasing with temperature T . This behavior is in stark contrast to resonant hole-exciton scattering, whose strong energy dependence is reflected in the T -dependence of resistivity, see Fig. 3. The behavior of the resistivity is divided into three regimes determined by the detuning Δ . The regimes can be understood from the scattering rate $\text{Im}\Sigma_h^R(p_F^h, 0)$ in Eq. (2) evaluated on the Fermi surface.

(i) At small temperatures $k_B T \ll \hbar^2 n_x/m_x$ and fixed exciton density, the boson chemical potential goes to zero: $\mu_x/k_B T \approx 0$. Away from resonance, $(\sqrt{\Delta} - \sqrt{\Delta_*})^2 \gg k_B T$, we find that $\text{Im}\Sigma_h^R(p_F^h, 0)$ decreases exponentially with $1/k_B T$ due to the conservation of energy and momentum.

(ii) At small temperatures $k_B T \ll \hbar^2 n_x/m_x$ but close to resonance, $(\sqrt{\Delta} - \sqrt{\Delta_*})^2 \ll k_B T$, excitons with en-

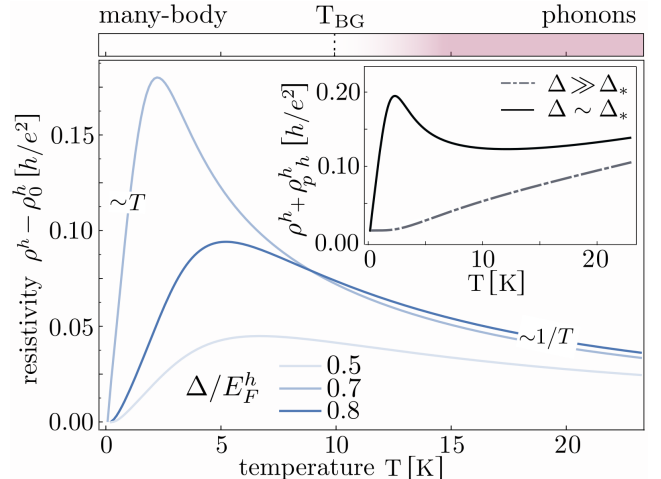


FIG. 3. Temperature dependence of the hole resistivity. Many-body contribution to the resistivity $\rho^h - \rho_0^h$ as a function of temperature T for different detunings Δ , where $\rho_0^h = 2\pi/\mu_h e^2 \tau_0$ is the Drude resistivity at zero temperature. Inset: Total resistivity $\rho^h + \rho_{\text{ph}}^h$ for $\Delta/E_F^h = 0.7$, including the contribution from scattering with acoustic phonons ρ_{ph}^h . Below the Bloch-Grüneisen temperature $T_{\text{BG}} \approx 10\text{K}$ (consistent with experiments [33, 34, 40]), exciton-charge scattering dominates over phonon scattering.

ergies $\omega_{\mathbf{k}} \ll T$ participate in the scattering. For these, $n_B(\omega_{\mathbf{k}}) \sim T/\omega_{\mathbf{k}}$ is large and dominates the momentum integral, yielding a dominant linear-in- T resistivity.

(iii) At high temperatures $k_B T \gg \hbar^2 n_x/m_x$, the exciton chemical potential is sizeable, and the dominant term in the scattering rate is $\text{Im}\Sigma_h^R(p_F^h, 0) \sim 1/k_B T$.

The many-body contribution dominates the hole resistivity below the Bloch-Grüneisen temperature $T_{\text{BG}} = 2\hbar v_s p_F^h$, where v_s is the speed of sound and p_F^h the hole Fermi momentum. At higher temperatures, acoustic phonons with momenta close to $2p_F^h$ are thermally excited and contribute as $\rho_{\text{ph}}^h = 2\pi/\mu_h e^2 \tau_{\text{ph}}^h$ to the resistivity, which increases linearly with T . The crossover to phonon-dominated scattering is shown in the inset of Fig. 3, where we have used τ_{ph}^h estimated in Ref. [44, 45].

Ac transport properties.— Having analyzed the Feshbach tunable transport of our Bose-Fermi mixture, we now focus on the ac response, see Fig. 4. Albeit challenging to measure experimentally at this point, the ac response provides us with insights in the underlying coupled transport mechanism. We find that the ac response can be effectively described by a simple three-fluid model in terms of the hydrodynamic variables $\mathbf{v}_h, \mathbf{v}_x, \mathbf{v}_t$, which identify as the velocities of the fluids [46].

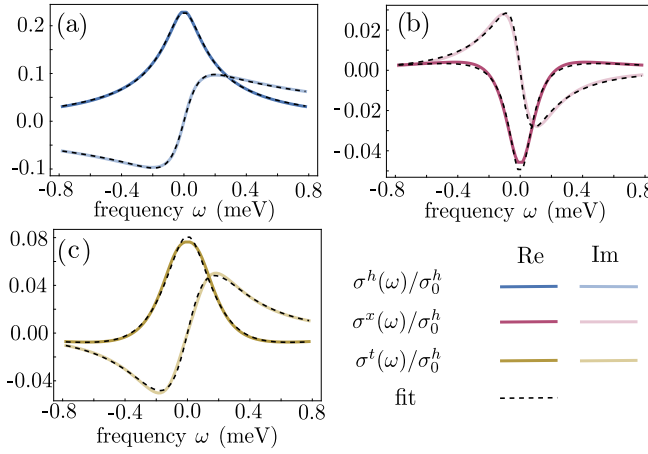


FIG. 4. **Ac conductivities.** Ac conductivity of (a) holes, (b) excitons and (c) trions, at $\Delta/E_F^h = 0.5$ and $T = 5.8$ K obtained from the kinetic approach (solid lines) and fitted to the three-fluid model (dashed lines).

$$\begin{aligned} \dot{\mathbf{v}}_h - \frac{e\mathbf{E}}{m_h} + \frac{\mathbf{v}_h}{\tau_h} &= -\alpha_{th} \frac{n_t}{m_h} (\mathbf{v}_h - \mathbf{v}_t) - \alpha_{xh} \frac{n_x}{m_h} (\mathbf{v}_h - \mathbf{v}_x), \\ \dot{\mathbf{v}}_x + \frac{\mathbf{v}_x}{\tau_x} &= -\alpha_{tx} \frac{n_t}{m_x} (\mathbf{v}_x - \mathbf{v}_t) - \alpha_{xh} \frac{n_h}{m_x} (\mathbf{v}_x - \mathbf{v}_h), \\ \dot{\mathbf{v}}_t + \frac{\mathbf{v}_t}{\tau_t} &= -\alpha_{th} \frac{n_h}{m_t} (\mathbf{v}_t - \mathbf{v}_h) - \alpha_{tx} \frac{n_x}{m_t} (\mathbf{v}_t - \mathbf{v}_x), \end{aligned}$$

where $\dot{\mathbf{v}}_i$ is the time derivative of \mathbf{v}_i . Three drag coefficients α_{ij} , with $i \neq j \in \{h, x, t\}$, model the effect of interactions in the Bose-Fermi mixture as “viscous friction forces.” The three momentum relaxation rates τ_i , for $i \in \{h, x, t\}$, model the many-body corrections to τ_0 . Only holes feel the longitudinal acceleration field $e\mathbf{E}/m_h$. The right hand side of the equations is the most general system of linear coupling terms which vanishes at $\mathbf{v}_h = \mathbf{v}_x = \mathbf{v}_t$ and preserves the total momentum $\mathbf{P} = \sum_i n_i m_i \mathbf{v}_i$ (i.e. they ensure $\dot{\mathbf{P}} = \mathbf{0}$ in the limit $\tau_i \rightarrow \infty$ and at $\mathbf{E} = \mathbf{0}$). Solving these equations, we obtain the ac conductivities from $n_i \mathbf{v}_i = \sigma^i \mathbf{E}/e$ as functions of six parameters $\tau_h, \tau_x, \tau_t, \alpha_{xh}, \alpha_{th}, \alpha_{tx}$ which are functions of Δ and T ; for instance, the sign-switching exciton drag coincides with a sign-switching drag coefficient $\alpha_{xh} \propto \text{sign}(\Delta - \Delta_*)$. A striking feature of the ac results is that the dissipative part of drag conductivities of excitons and trions $\text{Re}(\sigma^x), \text{Re}(\sigma^t)$ change their sign at a finite frequency set by the competition between drag forces and relaxation rates, highlighting the deviations from the Lorentz-shaped Drude behavior.

Outlook.— In this work we study tunable transport properties of a strongly-correlated Bose-Fermi mixtures realized in TMD heterostructures. As a result of the strong interactions near the solid-state Feshbach resonance, we predict an unconventional temperature dependence of the conductivities and a sign-changing exciton drag. Remarkably, selectively enhanced many-body scat-

tering dominates over other scattering channels such as disorder and phonons, provided the system is below the Bloch-Grüneisen temperature. Our results can guide future experiments and demonstrate the potential for TMD heterostructures to investigate strongly interacting Bose-Fermi mixtures, which appear in a variety of physical settings and often undergo interesting instabilities.

Our findings open exciting avenues for exploring the interplay between transport phenomena and pairing instabilities in Bose-Fermi mixtures allowed by exciton condensation. In fact, the low relative temperatures ($T/T_F \leq 0.01$) already achieved experimentally [15, 33, 34, 40] are promising for reaching regimes of exciton condensation. Phase fluctuations in the exciton gas are expected to play a significant role [9, 47], potentially leading to the emergence of unconventional phases [29, 31]. Furthermore, additional theoretical studies could provide insights into the hydrodynamic behavior of these quantum mixtures [48–50]. Another interesting direction for future work is to explore how the stability of Wigner crystals, realized in the low density regime of holes [51, 52], is modified by the presence of a finite exciton density.

Acknowledgments.— We thank Z. Hao, A. Imamoğlu, W. Kadow, and A. Mozes for fruitful discussions. We acknowledge support from the Deutsche Forschungsgemeinschaft (DFG, German Research Foundation) under Germany’s Excellence Strategy—EXC-2111-390814868, TRR 360 – 492547816 and DFG grants No. KN1254/1-2, KN1254/2-1, the European Research Council (ERC) under the European Union’s Horizon 2020 research and innovation programme (grant agreement No. 851161), as well as the Munich Quantum Valley, which is supported by the Bavarian state government with funds from the Hightech Agenda Bayern Plus. C.K. acknowledges funding from the Swiss National Science Foundation (Postdoc.Mobility Grant No. 217884).

Data availability.— Data and codes are available upon reasonable request on Zenodo [53].

Author contributions.— C.Z. and L.M. developed the kinetic theory. C.K. developed the Kubo formalism. C.Z. performed the numerical analysis. M.K. conceived the project. All authors contributed to the discussions of the results and the writing of the manuscript.

* These authors contributed equally to this work.

- [1] L. D. Landau, Über die bewegung der elektronen in kristallgitter, Phys. Z. Sowjetunion **3**, 134512 (1933).
- [2] S. Pekar, Autolocalization of the electron in an inertially polarizable dielectric medium, Zh. Eksp. Teor. Fiz. **16**, 335 (1946).
- [3] J. A. Hertz, Quantum critical phenomena, *Physical Review B* **14**, 1165–1184 (1976).
- [4] P. A. Lee, N. Nagaosa, and X.-G. Wen, Doping a mott in-

sulator: Physics of high-temperature superconductivity, *Reviews of Modern Physics* **78**, 17–85 (2006).

[5] H. v. Löhneysen, A. Rosch, M. Vojta, and P. Wölfle, Fermi-liquid instabilities at magnetic quantum phase transitions, *Reviews of Modern Physics* **79**, 1015–1075 (2007).

[6] S. Sachdev, *Quantum Phase Transitions* (Cambridge University Press, 2011).

[7] T. Li, S. Jiang, L. Li, Y. Zhang, K. Kang, J. Zhu, K. Watanabe, T. Taniguchi, D. Chowdhury, L. Fu, J. Shan, and K. F. Mak, Continuous mott transition in semiconductor moiré superlattices, *Nature* **597**, 350–354 (2021).

[8] T. Senthil, Theory of a continuous mott transition in two dimensions, *Phys. Rev. B* **78**, 045109 (2008).

[9] L. Ma, P. X. Nguyen, Z. Wang, Y. Zeng, K. Watanabe, T. Taniguchi, A. H. MacDonald, K. F. Mak, and J. Shan, Strongly correlated excitonic insulator in atomic double layers, *Nature* **598**, 585 (2021).

[10] I. Schwartz, Y. Shimazaki, C. Kuhlenkamp, K. Watanabe, T. Taniguchi, M. Kroner, and A. Imamoğlu, Electrically tunable feshbach resonances in twisted bilayer semiconductors, *Science* **374**, 336–340 (2021).

[11] H. Park, J. Zhu, X. Wang, Y. Wang, W. Holtzmann, T. Taniguchi, K. Watanabe, J. Yan, L. Fu, T. Cao, D. Xiao, D. R. Gamelin, H. Yu, W. Yao, and X. Xu, Dipole ladders with large Hubbard interaction in a moiré exciton lattice, *Nat. Phys.* **19**, 1286 (2023).

[12] R. Xiong, J. H. Nie, S. L. Brantly, P. Hays, R. Sailus, K. Watanabe, T. Taniguchi, S. Tongay, and C. Jin, Correlated insulator of excitons in WSe₂/WS₂ moiré superlattices, *Science* **380**, 860 (2023).

[13] B. Gao, D. G. Suárez-Forero, S. Sarkar, T.-S. Huang, D. Session, M. J. Mehrabad, R. Ni, M. Xie, P. Upadhyay, J. Vannucci, S. Mittal, K. Watanabe, T. Taniguchi, A. Imamoglu, Y. Zhou, and M. Hafezi, Excitonic Mott insulator in a Bose-Fermi-Hubbard system of moiré WS₂/WSe₂ heterobilayer, *Nat. Commun.* **15**, 1 (2024).

[14] Z. Lian, Y. Meng, L. Ma, I. Maity, L. Yan, Q. Wu, X. Huang, D. Chen, X. Chen, X. Chen, M. Blei, T. Taniguchi, K. Watanabe, S. Tongay, J. Lischner, Y.-T. Cui, and S.-F. Shi, Valley-polarized excitonic Mott insulator in WS₂/WSe₂ moiré superlattice, *Nat. Phys.* **20**, 34 (2024).

[15] P. X. Nguyen, R. Chaturvedi, L. Ma, P. Knuppel, K. Watanabe, T. Taniguchi, K. F. Mak, and J. Shan, A degenerate trion liquid in atomic double layers (2023), arXiv:2312.12571 [cond-mat.mes-hall].

[16] R. Qi, Q. Li, Z. Zhang, S. Chen, J. Xie, Y. Ou, Z. Cui, D. D. Dai, A. Y. Joe, T. Taniguchi, K. Watanabe, S. Tongay, A. Zettl, L. Fu, and F. Wang, Electrically controlled interlayer trion fluid in electron-hole bilayers (2023), arXiv:2312.03251 [cond-mat.mes-hall].

[17] P. Upadhyay, D. G. Suárez-Forero, T.-S. Huang, M. J. Mehrabad, B. Gao, S. Sarkar, D. Session, K. Watanabe, T. Taniguchi, Y. Zhou, M. Knap, and M. Hafezi, Giant enhancement of exciton diffusion near an electronic mott insulator (2024), arXiv:2409.18357 [cond-mat.str-el].

[18] A. B. Mhenni, W. Kadow, M. J. Metelski, A. O. Paulus, A. Dijkstra, K. Watanabe, T. Taniguchi, S. A. Tongay, M. Barbone, J. J. Finley, M. Knap, and N. P. Wilson, Gate-tunable bose-fermi mixture in a strongly correlated moiré bilayer electron system (2024), arXiv:2410.07308 [cond-mat.str-el].

[19] C. Chin, R. Grimm, P. Julienne, and E. Tiesinga, Feshbach resonances in ultracold gases, *Rev. Mod. Phys.* **82**, 1225 (2010).

[20] I. Bloch, J. Dalibard, and W. Zwerger, Many-body physics with ultracold gases, *Rev. Mod. Phys.* **80**, 885 (2008).

[21] I. Ferrier-Barbut, M. Delehaye, S. Laurent, A. T. Grier, M. Pierce, B. S. Rem, F. Chevy, and C. Salomon, A mixture of bose and fermi superfluids, *Science* **345**, 1035 (2014).

[22] B. J. DeSalvo, K. Patel, G. Cai, and C. Chin, Observation of fermion-mediated interactions between bosonic atoms, *Nature* **568**, 61 (2019).

[23] Z. Z. Yan, Y. Ni, A. Chuang, P. E. Dolgirev, K. Seetharam, E. Demler, C. Robens, and M. Zwierlein, Collective flow of fermionic impurities immersed in a bose-einstein condensate, *Nature Physics* **20**, 1395–1400 (2024).

[24] M. Duda, X.-Y. Chen, A. Schindewolf, R. Bause, J. von Milczewski, R. Schmidt, I. Bloch, and X.-Y. Luo, Transition from a polaronic condensate to a degenerate fermi gas of heteronuclear molecules, *Nature Physics* **19**, 720 (2023).

[25] N. P. Wilson, W. Yao, J. Shan, and X. Xu, Excitons and emergent quantum phenomena in stacked 2d semiconductors, *Nature* **599**, 383 (2021).

[26] M. Sidler, P. Back, O. Cotlet, A. Srivastava, T. Fink, M. Kroner, E. Demler, and A. Imamoglu, Fermi polaron-polaritons in charge-tunable atomically thin semiconductors, *Nature Physics* **13**, 255 (2017).

[27] C. Fey, P. Schmelcher, A. Imamoglu, and R. Schmidt, Theory of exciton-electron scattering in atomically thin semiconductors, *Phys. Rev. B* **101**, 195417 (2020).

[28] C. Kuhlenkamp, M. Knap, M. Wagner, R. Schmidt, and A. Imamoğlu, Tunable feshbach resonances and their spectral signatures in bilayer semiconductors, *Phys. Rev. Lett.* **129**, 037401 (2022).

[29] C. Zerba, C. Kuhlenkamp, A. Imamoğlu, and M. Knap, Realizing topological superconductivity in tunable bose-fermi mixtures with transition metal dichalcogenide heterostructures, *Phys. Rev. Lett.* **133**, 056902 (2024).

[30] J. von Milczewski, X. Chen, A. Imamoglu, and R. Schmidt, Superconductivity induced by strong electron-exciton coupling in doped atomically thin semiconductor heterostructures, *Phys. Rev. Lett.* **133**, 226903 (2024).

[31] A. Kumar, A. S. Patri, and T. Senthil, Unconventional superconductivity mediated by exciton density wave fluctuations (2024), arXiv:2410.09148 [cond-mat.str-el].

[32] V. Crépel, D. Guerci, J. Cano, J. H. Pixley, and A. Millis, Topological superconductivity in doped magnetic moiré semiconductors, *Phys. Rev. Lett.* **131**, 056001 (2023).

[33] A. Y. Joe, K. Pistunova, K. Kaasbjerg, K. Wang, B. Kim, D. A. Rhodes, T. Taniguchi, K. Watanabe, J. Hone, T. Low, L. A. Jauregui, and P. Kim, Transport study of charge-carrier scattering in monolayer wse₂, *Phys. Rev. Lett.* **132**, 056303 (2024).

[34] J. Pack, Y. Guo, Z. Liu, B. S. Jessen, L. Holtzman, S. Liu, M. Cothrine, K. Watanabe, T. Taniguchi, D. G. Mandrus, K. Barmak, J. Hone, and C. R. Dean, Charge-transfer contacts for the measurement of correlated states in high-mobility WSe₂, *Nat. Nanotechnol.* **19**, 948 (2024).

[35] Z. Wang, D. A. Rhodes, K. Watanabe, T. Taniguchi,

J. C. Hone, J. Shan, and K. F. Mak, Evidence of high-temperature exciton condensation in two-dimensional atomic double layers, *Nature* **574**, 76 (2019).

[36] See Supplemental Material.

[37] S. Powell, S. Sachdev, and H. P. Büchler, Depletion of the bose-einstein condensate in bose-fermi mixtures, *Phys. Rev. B* **72**, 024534 (2005).

[38] A. Kormányos, G. Burkard, M. Gmitra, J. Fabian, V. Zólyomi, N. D. Drummond, and V. Fal'ko, $k \cdot p$ theory for two-dimensional transition metal dichalcogenide semiconductors, *2D Materials* **2**, 022001 (2015).

[39] L. A. Jauregui, A. Y. Joe, K. Pistunova, D. S. Wild, A. A. High, Y. Zhou, G. Scuri, K. De Greve, A. Sushko, C.-H. Yu, T. Taniguchi, K. Watanabe, D. J. Needelman, M. D. Lukin, H. Park, and P. Kim, Electrical control of interlayer exciton dynamics in atomically thin heterostructures, *Science* **366**, 870 (2019).

[40] Y. Guo, J. Pack, J. Swann, L. Holtzman, M. Cothrine, K. Watanabe, T. Taniguchi, D. G. Mandrus, K. Barmak, J. Hone, A. J. Millis, A. N. Pasupathy, and C. R. Dean, Superconductivity in 5.0° twisted bilayer wse2, *Nature* **637**, 839 (2025).

[41] A. Kamenev, *Field Theory of Non-Equilibrium Systems* (Cambridge University Press, Cambridge, England, UK, 2011).

[42] G. D. Mahan, *Many-Particle Physics* (Springer US).

[43] O. Cotlet, F. Pientka, R. Schmidt, G. Zarand, E. Demler, and A. Imamoğlu, Transport of neutral optical excitations using electric fields, *Phys. Rev. X* **9**, 041019 (2019).

[44] A. Lavasani, D. Bulmash, and S. Das Sarma, Wiedemann-franz law and fermi liquids, *Phys. Rev. B* **99**, 085104 (2019).

[45] Y. Huang and S. Das Sarma, Electronic transport, metal-insulator transition, and wigner crystallization in transition metal dichalcogenide monolayers, *Phys. Rev. B* **109**, 245431 (2024).

[46] Formally, they are defined, for $i \in \{h, x, t\}$, by $\mathbf{v}_i(\mathbf{r}) = \int \frac{d^2\mathbf{q}}{(2\pi)^2} \frac{\mathbf{q}}{m_i} f_i(\mathbf{r}, \mathbf{q})/n_i(\mathbf{r})$ where f_i is the quasi-particle distribution function in phase space and $n_i = \int \frac{d^2\mathbf{q}}{(2\pi)^2} f_i$.

[47] O. Cotlet, S. Zeytinoğlu, M. Sigrist, E. Demler, and A. m. c. Imamoğlu, Superconductivity and other collective phenomena in a hybrid bose-fermi mixture formed by a polariton condensate and an electron system in two dimensions, *Phys. Rev. B* **93**, 054510 (2016).

[48] A. Levchenko and J. Schmalian, Transport properties of strongly coupled electron-phonon liquids, *Annals of Physics* **419**, 168218 (2020).

[49] X. Huang and A. Lucas, Electron-phonon hydrodynamics, *Phys. Rev. B* **103**, 155128 (2021).

[50] L. Fritz and T. Scaffidi, Hydrodynamic electronic transport, *Annual Review of Condensed Matter Physics* **15**, 17 (2024).

[51] T. Smoleński, P. E. Dolgirev, C. Kuhlenkamp, A. Popert, Y. Shimazaki, P. Back, X. Lu, M. Kroner, K. Watanabe, T. Taniguchi, I. Esterlis, E. Demler, and A. Imamoğlu, Signatures of wigner crystal of electrons in a monolayer semiconductor, *Nature* **595**, 53 (2021).

[52] Y. Zhou, J. Sung, E. Brutschea, I. Esterlis, Y. Wang, G. Scuri, R. J. Gelly, H. Heo, T. Taniguchi, K. Watanabe, G. Zaránd, M. D. Lukin, P. Kim, E. Demler, and H. Park, Bilayer wigner crystals in a transition metal dichalcogenide heterostructure, *Nature* **595**, 48 (2021).

[53] C. Zerba, C. Kuhlenkamp, L. Mangeolle, and M. Knap, Tuning transport in solid-state Bose-Fermi mixtures by Feshbach resonances (2024).

[54] C. Kuhlenkamp, M. Knap, M. Wagner, R. Schmidt, and A. Imamoğlu, Tunable feshbach resonances and their spectral signatures in bilayer semiconductors, *Phys. Rev. Lett.* **129**, 037401 (2022).

[55] H. T. Stoof, K. B. Gubbels, and D. Dickerscheid, *Ultracold quantum fields* (Springer, 2009).

[56] W. Zwerger, Strongly interacting fermi gases, in *Proceedings of the International School of Physics "Enrico Fermi" - Course 191 "Quantum Matter at Ultralow Temperatures"*, edited by M. Inguscio, W. Ketterle, S. Stringari, and G. Roati (IOS Press, Amsterdam; SIF Bologna, 2016) pp. 63–142.

[57] J. Rammer, *Quantum Transport Theory* (Taylor & Francis, Andover, England, UK, 2019).

[58] G. Baym and L. P. Kadanoff, Conservation laws and correlation functions, *Physical Review* **124**, 287–299 (1961).

Microscopic model

Here we derive the effective model of the main text from a microscopic Hamiltonian which describes the scattering between holes and excitons across different layers:

$$\hat{H} = \sum_{\mathbf{k}} x_{\mathbf{k}}^\dagger \frac{k^2}{2m_x} x_{\mathbf{k}} + \begin{pmatrix} c_{\mathbf{k},T}^\dagger \\ c_{\mathbf{k},M}^\dagger \end{pmatrix} \begin{pmatrix} \frac{k^2}{2m} + \Delta & t \\ t & \frac{k^2}{2m} \end{pmatrix} \begin{pmatrix} c_{\mathbf{k},T} \\ c_{\mathbf{k},M} \end{pmatrix} + \frac{U}{V} \sum_{\mathbf{k}, \mathbf{k}', \mathbf{q}} c_{\mathbf{k},M}^\dagger c_{\mathbf{k}+\mathbf{q},M} x_{\mathbf{k}'}^\dagger x_{\mathbf{k}'-\mathbf{q}}, \quad (5)$$

where the indices $\{T, M\}$ label the top and middle layers, t is the amplitude for doped holes tunneling from the top layer to the middle layer, and we assume contact interactions of strength U between interlayer excitons and middle-layer holes.

Scattering between excitons and holes is described by going to the center-of-mass frame, in which the wavefunction at energy $E = \mathbf{k}^2/2m_{\text{red}}$ takes the following form

$$\psi_{\mathbf{k}}(\mathbf{r}) = e^{i\mathbf{k}\mathbf{r}} + f(\mathbf{k}) \sqrt{\frac{i}{8\pi}} \frac{e^{i|\mathbf{k}|\mathbf{r}}}{\sqrt{|\mathbf{r}||\mathbf{k}|}}, \quad (6)$$

where \mathbf{k} denotes the relative momentum, $e^{i\mathbf{k}\mathbf{r}}$ is an incoming plane wave and the last term describes the outgoing spherical wave after scattering. Eq. (6) defines a dimensionless scattering amplitude $f(\mathbf{k})$, which is related to the cross-section $d\sigma/d\theta$ via

$$\frac{d\sigma}{d\theta}(\mathbf{k}) = \frac{|f(\mathbf{k})|^2}{8\pi|\mathbf{k}|}. \quad (7)$$

One can also relate $f(\mathbf{k})$ to the T-matrix, by analyzing the Lippmann-Schwinger equation for the scattering state $|\psi_{\mathbf{k}}^+\rangle$ (identified with $\psi_{\mathbf{k}}(\mathbf{r})$ in Eq. (6)):

$$|\psi_{\mathbf{k}}^+\rangle = |\mathbf{k}\rangle + G_0 \hat{H}_{xh} |\psi_{\mathbf{k}}^+\rangle = |\mathbf{k}\rangle + G_0 \hat{T} |\mathbf{k}\rangle, \quad (8)$$

where \hat{H}_{xh} is the interaction term corresponding to the second line of Eq. (5) and $\langle \mathbf{r}|G_0|\mathbf{r}'\rangle = \int \frac{d^2 k}{(2\pi)^2} \frac{e^{i\mathbf{k}(\mathbf{r}-\mathbf{r}')}}{E+i0^+-\mathbf{k}^2/2m_{\text{red}}}$. Expanding Eq. (8) for large $|\mathbf{r}|$ establishes the relation between \hat{T} and $f(\mathbf{k})$:

$$f(\mathbf{k}) = -2m_{\text{red}} T(\mathbf{k}^2/2m_{\text{red}}). \quad (9)$$

This defines the dimensionless $f(E) = f(\mathbf{k})|_{\mathbf{k}^2/2m_{\text{red}}=E}$ in Fig. 1 of the main text.

Starting from Eq.(5), the hole-exciton T-matrix is obtained by solving the Bethe-Selpeiter equation depicted in Fig. 5 (b), and reads $T = \frac{t^2}{U^{-1}-\Xi_{xh}} G_{h,M}^2$, where $G_{h,M}$ is the propagator of holes in the middle layer and Ξ_{xh} is the exciton-hole bubble. Since Ξ_{xh} is UV divergent, we regularize the theory by introducing a momentum cut-off and renormalizing U such that the model reproduces the experimental value of the inter-layer trion binding

energy E_t^0 (see Ref. [54]). Near a Feshbach resonance, the scattering process is predominantly governed by this interlayer trion, which yields the following T-matrix near resonance:

$$T(\omega) \simeq -\frac{2\pi}{m_{\text{red}}\Delta^2 \log((\omega - \Delta)/E_t^0)} t^2 \quad (10a)$$

$$\simeq \frac{2\pi|E_t^0|}{m_{\text{red}}\Delta^2(\omega - E_t^0 + \Delta + i0^+)} t^2. \quad (10b)$$

The microscopic T-matrix near resonance is found to have a pole at the energy of the molecule. Consequently, we can consider an effective model where the scattering between excitons and top-layer electrons is mediated by a virtual trion. The elementary scattering event of the effective model, represented by the diagram in Fig. 5 (a), is described by an effective T-matrix T_{eff} , which has a pole at the trion energy:

$$T_{\text{eff}}(\omega) \approx \frac{g^2}{\omega - E_t^0 + \Delta + i0^+}, \quad (11)$$

see also Refs. [29, 55, 56]. The coupling parameter g is the effective hole-exciton-molecule vertex. By matching the effective T-matrix T_{eff} to second order in g with the full T-matrix T , we can derive an expression for g ,

$$g = \left(\frac{2\pi}{m_{\text{red}} E_t^0} \right)^{\frac{1}{2}} t, \quad (12)$$

which is the effective three-body coupling of Eq. (1).

Kinetic equations

Derivation.— Starting from the Hamiltonian Eq. (1), we derive a set of three coupled Boltzmann equations,

$$\left(\partial_t + \mathbf{v}_i \cdot \partial_{\mathbf{r}} + \mathbf{f}_i \cdot \partial_{\mathbf{q}} \right) F_i = I_i [F_h, F_x, F_t], \quad (13)$$

for the three species of particles, $i \in \{h, x, t\}$, holes, excitons, trions, respectively. These equations provide a semiclassical approximation of the dynamics of the system out of equilibrium, where $F_i(\mathbf{r}, \mathbf{q}, t)$ are the quasi-particle mass-shell distribution functions in phase space (at position \mathbf{r} and momentum \mathbf{q}), to be determined. On the left-hand side, $\mathbf{f}_i(\mathbf{r}, \mathbf{q})$ is the force acting on a particle and $\mathbf{v}_i(\mathbf{r}, \mathbf{q})$ is the particle's velocity. The right-hand side I_i is the collision integral, which accounts for the effect of out-of-equilibrium many-body scattering as well as incoherent background scattering arising for example from impurities.

We use the real-time formalism for nonequilibrium field theory [41, 57] to obtain the hole-exciton-trion contribution to the kinetic equations Eq. (13). This involves defining the quantum action along a closed time contour going forward from $t = -\infty$ to $t = +\infty$, then backward

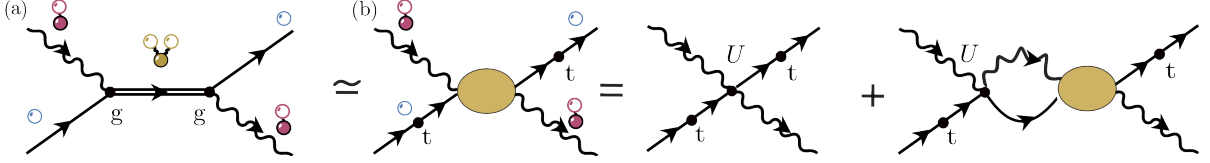


FIG. 5. **Diagrammatic derivation of the effective model.** **a)** T-matrix T_{eff} for the effective interaction between hole, exciton and trion. **b)** The T-matrix T of the microscopic model is given by the solution of the Bethe-Salpeter equation; at leading order and near the Feshbach resonance, it is equivalent to the T-matrix T_{eff} of the effective model.

from $t = +\infty$ to $t = -\infty$, and for each a different set of quantum fields. In coherent state notations where $\bar{x}, \bar{h}, \bar{t}$ represent the conjugate fields of x, h, t respectively, we thus introduce $x^\pm, \bar{x}^\pm, h^\pm, \bar{h}^\pm, t^\pm, \bar{t}^\pm$ where $+$ labels operators appearing in the forward-time integral, and $-$ in the backward-time integral. We recall the Keldysh rotation for a bosonic field x

$$x_{cl/q}(t) = (x^+(t) \pm x^-(t))/\sqrt{2}, \quad (14a)$$

$$\bar{x}_{cl/q}(t) = (\bar{x}^+(t) \pm \bar{x}^-(t))/\sqrt{2}, \quad (14b)$$

where $+$ is for “cl” and $-$ for “q” in \pm , while for a fermionic field f (here $f = h, t$)

$$f_{r/a}(t) = (f^+(t) \pm f^-(t))/\sqrt{2}, \quad (15a)$$

$$\bar{f}_{r/a}(t) = (\bar{f}^+(t) \mp \bar{f}^-(t))/\sqrt{2}, \quad (15b)$$

where $+$ is for “r” and $-$ for “a” in the first line and conversely in the second. The action for the free fields ($f = h, t$) reads

$$S_{x,0} = \sum_{\mathbf{k}, \mathbf{k}'} \int dt \begin{bmatrix} \bar{x}^{cl} \\ \bar{x}^q \end{bmatrix}_{\mathbf{k}}^\top \begin{bmatrix} 0 & [G_{x,0}^{-1}]^A \\ [G_{x,0}^{-1}]^R & [G_{x,0}^{-1}]^K \end{bmatrix}_{\mathbf{k}, \mathbf{k}'} \begin{bmatrix} x^{cl} \\ x^q \end{bmatrix}_{\mathbf{k}'}, \quad (16)$$

$$S_{f,0} = \sum_{\mathbf{p}, \mathbf{p}'} \int dt \begin{bmatrix} \bar{f}^r \\ \bar{f}^a \end{bmatrix}_{\mathbf{p}}^\top \begin{bmatrix} [G_{b,0}^{-1}]^R & [G_{b,0}^{-1}]^K \\ 0 & [G_{b,0}^{-1}]^A \end{bmatrix}_{\mathbf{p}, \mathbf{p}'} \begin{bmatrix} f^r \\ f^a \end{bmatrix}_{\mathbf{p}'}. \quad (17)$$

Here and in the following, time integrals are defined along the forward contour.

Eqs. (16), (17) involve the free (retarded and advanced) bosonic propagator $[G_{x,0}^{R/A}]_{\mathbf{k}, \mathbf{k}'}(E) = \frac{\delta_{\mathbf{k}, \mathbf{k}'}^+}{E - \omega_{\mathbf{k}} \pm i0^+}$ and fermionic propagator $[G_{f,0}^{R/A}]_{\mathbf{p}, \mathbf{p}'}(E) = \frac{\delta_{\mathbf{p}, \mathbf{p}'}^+}{E - \epsilon_{f, \mathbf{p}} \pm i0^+}$, where $+$ is for “R” and $-$ is for “A” in \pm .

The free Keldysh propagators are for bosons $[G_{x,0}^K]_{\mathbf{k}, \mathbf{k}'}(E) = -2i\pi F_x(\mathbf{k}, E)\delta(E - \omega_{\mathbf{k}})\delta_{\mathbf{k}, \mathbf{k}'}$ and for fermions $[G_{f,0}^K]_{\mathbf{p}, \mathbf{p}'}(E) = -2i\pi F_f(\mathbf{p}, E)\delta(E - \epsilon_{f, \mathbf{p}})\delta_{\mathbf{p}, \mathbf{p}'}$; at this stage $F_i(\mathbf{q}, E)$ are just parameter functions.

The interacting part of the action, in terms of the

Keldysh-rotated fields, reads

$$S_{int} = -\frac{g}{\sqrt{2N}} \int dt \sum_{\mathbf{k}, \mathbf{p}} \left(x_{\mathbf{k}}^{cl} \bar{t}_{\mathbf{p}+\mathbf{k}}^a h_{\mathbf{p}}^a + x_{\mathbf{k}}^{cl} \bar{t}_{\mathbf{p}+\mathbf{k}}^r h_{\mathbf{p}}^r + x_{\mathbf{k}}^q \bar{t}_{\mathbf{p}+\mathbf{k}}^a h_{\mathbf{p}}^r + x_{\mathbf{k}}^q \bar{t}_{\mathbf{p}+\mathbf{k}}^r h_{\mathbf{p}}^a \right) + \text{h.c.}, \quad (18)$$

where “+ h.c.” means conjugating all fields (in the coherent state path integral sense), exchanging r/a and commuting the fermionic Grassmann fields. Here N is the total number of unit cells in a layer, and in the following A will be the total area of a layer.

From Eq. (18), the self-energies can be obtained perturbatively from Dyson’s equation,

$$\mathbf{G}_i(t, t') = \mathbf{G}_{0,i}(t - t') \quad (19)$$

$$+ \int \int dt_1 dt_2 \mathbf{G}_{0,i}(t - t_1) \mathbf{\Sigma}_i(t_1, t_2) \mathbf{G}_i(t_2 - t'),$$

for $i \in h, x, t$ and where all quantities $\mathbf{G}_i, \mathbf{G}_{0,i}, \mathbf{\Sigma}_i$ have a matrix structure in momentum space (i.e. they are functions of two momentum variables) and in Keldysh space (they have a 2×2 structure with indices {cl,q} for the bosons and {r,a} for the fermions). The interacting theory retains the same matrix structure as the free theory, thus defining retarded, advanced and Keldysh self energies [41, 57]; for bosons $\Sigma_x^R = \Sigma_x^{q, cl}$, $\Sigma_x^A = \Sigma_x^{q, a}$, $\Sigma_x^K = \Sigma_x^{q, q}$, and for fermions $\Sigma_f^R = \Sigma_f^{r, r}$, $\Sigma_f^A = \Sigma_f^{r, a}$, $\Sigma_f^K = \Sigma_f^{r, a}$ where $f \in \{h, t\}$.

The kinetic theory is obtained as a semiclassical approximation of the time evolution equations in phase space. This is obtained by computing the Wigner transform of the self-energy,

$$\Sigma_i(\mathbf{R}, t; \mathbf{k}, E) = \int dt' e^{iEt'} \sum_{\mathbf{k}'} e^{i\mathbf{k}' \cdot \mathbf{R}} \times \Sigma_i(\mathbf{k} + \frac{\mathbf{k}'}{2}, \mathbf{k} - \frac{\mathbf{k}'}{2}, t + \frac{t'}{2}, t - \frac{t'}{2}), \quad (20)$$

where \mathbf{R}, t are the “slow” space and time variables, and \mathbf{k}, E are the “fast” momentum and energy variables. To the perturbative order $O(g^2)$, we find

$$\Sigma_x^{R/A}(\mathbf{k}, E) = \frac{g^2}{2A} \sum_{\mathbf{p}} \frac{F_t(\mathbf{p} + \mathbf{k}) - F_h(\mathbf{p})}{E - \epsilon_{t, \mathbf{p}+\mathbf{k}} + \epsilon_{h, \mathbf{p}} \pm i0}, \quad (21a)$$

$$\Sigma_h^{R/A}(\mathbf{p}, E) = -\frac{g^2}{2A} \sum_{\mathbf{k}} \frac{F_t(\mathbf{k} + \mathbf{p}) - F_x(\mathbf{k})}{E + \omega_{\mathbf{k}} - \epsilon_{t, \mathbf{k}+\mathbf{p}} \pm i0}, \quad (21b)$$

$$\Sigma_t^{R/A}(\mathbf{p}, E) = \frac{g^2}{2A} \sum_{\mathbf{k}} \frac{F_x(\mathbf{k}) + F_h(\mathbf{p} - \mathbf{k})}{E - \omega_{\mathbf{k}} - \epsilon_{h, \mathbf{p}-\mathbf{k}} \pm i0}, \quad (21c)$$

where $+$ is for R and $-$ is for A in \pm , and

$$\Sigma_x^K(\mathbf{k}, E) = -\frac{i\pi g^2}{A} \sum_{\mathbf{p}} \left(1 - F_t(\mathbf{p} + \mathbf{k}) F_h(\mathbf{p}) \right) \times \times \delta(E - \epsilon_{t,\mathbf{p}+\mathbf{k}} + \epsilon_{h,\mathbf{p}}), \quad (22a)$$

$$\Sigma_h^K(\mathbf{p}, E) = \frac{i\pi g^2}{A} \sum_{\mathbf{k}} \left(1 - F_t(\mathbf{k} + \mathbf{p}) F_x(\mathbf{k}) \right) \times \times \delta(E + \omega_{\mathbf{k}} - \epsilon_{t,\mathbf{k}+\mathbf{p}}), \quad (22b)$$

$$\Sigma_t^K(\mathbf{p}, E) = -\frac{i\pi g^2}{A} \sum_{\mathbf{k}} (F_x(\mathbf{k}) F_h(\mathbf{p} - \mathbf{k}) + 1) \times \times \delta(E - \omega_{\mathbf{k}} - \epsilon_{\mathbf{p}-\mathbf{k}}). \quad (22c)$$

In Eqs. (21a)–(22c) and all the following, we keep im-

plicit the dependence of distributions F_i on the slow variables \mathbf{R}, t . The collision integral is obtained from the the Wigner transform of the self-energy as

$$\tilde{I}_i(\mathbf{q}) = i\Sigma_i^K(\mathbf{q}, \xi_{i,\mathbf{q}}) + 2\text{Im}\Sigma_i^R(\mathbf{q}, \xi_{i,\mathbf{q}})F_i(\mathbf{q}, \xi_{i,\mathbf{q}}), \quad (23)$$

with the shorthand $\xi_{x,\mathbf{q}} = \omega_{\mathbf{q}}$ and $\xi_{f,\mathbf{q}} = \epsilon_{f,\mathbf{q}}$. In general $F_i(\mathbf{q}, E)$ is a function of energy and momentum independently, however in Eq. (23) the energy variable is locked to the particle dispersion: this is a semiclassical approximation which relies on the existence of well-defined quasi-particles and allows one to write simply $F_i(\mathbf{q})$ where the on-shell energy argument $\xi_{i,\mathbf{q}}$ is implicit.

Inserting Eqs. (21a)–(22c) into Eq. (23) gives

$$\tilde{I}_x = \frac{g^2\pi}{A} \sum_{\mathbf{p}} \delta(\omega_{\mathbf{k}} - \epsilon_{t,\mathbf{p}+\mathbf{k}} + \epsilon_{h,\mathbf{p}}) \left[(1 - F_t(\mathbf{p} + \mathbf{k}) F_h(\mathbf{p})) + (F_h(\mathbf{p}) - F_t(\mathbf{p} + \mathbf{k})) F_x(\mathbf{k}) \right], \quad (24a)$$

$$\tilde{I}_h = -\frac{g^2\pi}{A} \sum_{\mathbf{k}} \delta(\omega_{\mathbf{k}} - \epsilon_{t,\mathbf{k}+\mathbf{p}} + \epsilon_{h,\mathbf{p}}) \left[(1 - F_t(\mathbf{k} + \mathbf{p}) F_x(\mathbf{k})) + (F_x(\mathbf{k}) - F_t(\mathbf{k} + \mathbf{p})) F_h(\mathbf{p}) \right], \quad (24b)$$

$$\tilde{I}_t = \frac{g^2\pi}{A} \sum_{\mathbf{k}} \delta(\omega_{\mathbf{k}} + \epsilon_{h,\mathbf{p}-\mathbf{k}} - \epsilon_{t,\mathbf{p}}) \left[(1 + F_x(\mathbf{k}) F_h(\mathbf{p} - \mathbf{k})) - (F_x(\mathbf{k}) + F_h(\mathbf{p} - \mathbf{k})) F_t(\mathbf{p}) \right]. \quad (24c)$$

These collision integrals satisfy detailed balance: they vanish when F_i are replaced by their equilibrium values $F_x^{\text{eq}}(\mathbf{k}) = 1 + 2n_B(\omega_{\mathbf{k}})$ and $F_h^{\text{eq}}(\mathbf{p}) = 1 - 2n_F(\epsilon_{h,\mathbf{p}})$ and $F_t^{\text{eq}}(\mathbf{p}) = 1 - 2n_F(\epsilon_{t,\mathbf{p}})$. Thus \tilde{I}_i capture interaction effects out of equilibrium, however they preserve total momentum [58] and do not account for current relaxation. In other words, \tilde{I}_i may capture drag effects but not diffusive transport. We then include momentum relaxation for all three species in the relaxation time approximation, at the rates $\tau_{h,\mathbf{p}}, \tau_{x,\mathbf{k}}, \tau_{t,\mathbf{p}}$. Such a collision term can arise from incoherent background scattering, for instance due to impurities. Thus, in Eq. (13) we take $I_i[F_h, F_x, F_t] = \tilde{I}_i[F_h, F_x, F_t] - (F_i - F_i^{\text{eq}})/\tau_i$.

Besides, in Eq. (13) all the energies, velocities and quasiparticle weights are in principle renormalized by interactions. However, such corrections are always higher order in powers of g^2 or τ_0/E_F^h than our level of approximation, thus we neglect such corrections and use the bare dispersions $\omega_{\mathbf{k}}, \epsilon_{h,\mathbf{p}}, \epsilon_{t,\mathbf{p}}$ and velocities $\mathbf{v}_x(\mathbf{k}) = \partial_{\mathbf{k}}\omega(\mathbf{k})$, $\mathbf{v}_h(\mathbf{p}) = \partial_{\mathbf{p}}\epsilon_h(\mathbf{p})$, $\mathbf{v}_t(\mathbf{k}) = \partial_{\mathbf{p}}\epsilon_t(\mathbf{p})$. In the setup we consider, the electric field \mathbf{E} applies solely to the holes, thus $\mathbf{f}_{h,\mathbf{p}} = e\mathbf{E}$ and $\mathbf{f}_{x,\mathbf{k}} = 0 = \mathbf{f}_{t,\mathbf{p}} = 0$. We furthermore assume a homogenous system (where temperature

and chemical potentials are uniform), so that all gradient terms vanish in equilibrium, $\mathbf{v}_i \partial_{\mathbf{r}} F_i^{\text{eq}} = 0$.

Solution.— We proceed by linearizing the kinetic equations Eq. (13) around equilibrium. We parameterize the non-equilibrium distributions as $F_x(\mathbf{k}) = F_x^{\text{eq}}(\mathbf{k}) + 2\varphi_x(\mathbf{k})$ and $F_h(\mathbf{p}) = F_h^{\text{eq}}(\mathbf{p}) - 2\varphi_h(\mathbf{p})$ and $F_t(\mathbf{p}) = F_t^{\text{eq}}(\mathbf{p}) - 2\varphi_t(\mathbf{p})$ for excitons, holes and trions respectively, n_B, n_F are the Bose and Fermi functions, and $\varphi_h, \varphi_x, \varphi_t$ are the deviations from equilibrium of the particle populations. From these, the conductivities are then defined as

$$\sigma^i(\Omega)\mathbf{E} = e \int \frac{d^2\mathbf{k}}{(2\pi)^2} \mathbf{v}_i(\mathbf{k}) \varphi_i(\mathbf{k}) \quad (25)$$

for $i \in h, x, t$. The linear response of the system to the external electric field is obtained by performing this replacement in the collision integral, while simply replacing F_i by F_i^{eq} on the left-hand side, except for the partial time derivative term which we write, in ac notations, as $i\Omega(F_i - F_i^{\text{eq}})$. As a result, we obtain the set of three coupled algebraic equations

$$\begin{aligned} \left(\frac{1}{\tau_{x,\mathbf{k}}} + i\Omega \right) \varphi_x(\mathbf{k}) &= \frac{2\pi}{A} g^2 \sum_{\mathbf{p}} \delta(\omega_{\mathbf{k}} - \epsilon_{t,\mathbf{p}+\mathbf{k}} + \epsilon_{h,\mathbf{p}}) \left[(n_F(\epsilon_{t,\mathbf{p}+\mathbf{k}}) - n_F(\epsilon_{h,\mathbf{p}})) \varphi_x(\mathbf{k}) \right. \\ &\quad \left. + (n_B(\omega_{\mathbf{k}}) - n_F(\epsilon_{h,\mathbf{p}}) + 1) \varphi_t(\mathbf{p} + \mathbf{k}) - (n_F(\epsilon_{t,\mathbf{p}+\mathbf{k}}) + n_B(\omega_{\mathbf{k}})) \varphi_h(\mathbf{p}) \right], \end{aligned} \quad (26a)$$

$$\begin{aligned} \left(\frac{1}{\tau_{h,\mathbf{k}}} + i\Omega \right) \varphi_h(\mathbf{p}) &= \frac{2\pi}{A} g^2 \sum_{\mathbf{k}} \delta(\omega_{\mathbf{k}} + \epsilon_{h,\mathbf{p}} - \epsilon_{t,\mathbf{p}+\mathbf{k}}) \left[\varphi_x(\mathbf{k}) (n_F(\epsilon_{t,\mathbf{k}+\mathbf{p}}) - n_F(\epsilon_{h,\mathbf{p}})) \right. \\ &\quad \left. + \varphi_t(\mathbf{k} + \mathbf{p}) (n_B(\omega_{\mathbf{k}}) - n_F(\epsilon_{h,\mathbf{p}}) + 1) - \varphi_h(\mathbf{p}) (n_B(\omega_{\mathbf{k}}) + n_F(\epsilon_{t,\mathbf{p}+\mathbf{k}})) \right] - (f_{h,\mathbf{p}} \cdot \partial_{\mathbf{p}}) n_F(\epsilon_{h,\mathbf{p}}), \end{aligned} \quad (26b)$$

$$\begin{aligned} \left(\frac{1}{\tau_{t,\mathbf{p}}} + i\Omega \right) \varphi_t(\mathbf{p}) &= \frac{2\pi}{A} g^2 \sum_{\mathbf{k}} \delta(\omega_{\mathbf{k}} + \epsilon_{h,\mathbf{p}-\mathbf{k}} - \epsilon_{t,\mathbf{p}}) \left[\varphi_x(\mathbf{k}) (n_F(\epsilon_{h,\mathbf{p}-\mathbf{k}}) - n_F(\epsilon_{t,\mathbf{p}})) \right. \\ &\quad \left. - \varphi_t(\mathbf{p}) (n_B(\omega_{\mathbf{k}}) - n_F(\epsilon_{h,\mathbf{p}-\mathbf{k}}) + 1) + \varphi_h(\mathbf{p} - \mathbf{k}) (n_B(\omega_{\mathbf{k}}) + n_F(\epsilon_{t,\mathbf{p}})) \right]. \end{aligned} \quad (26c)$$

In what follows, we use matrix notations for objects that are function of two momenta. In particular, we define the vector $\mathcal{K}_{\mathbf{p}}^h = (f_{h,\mathbf{p}} \cdot \partial_{\mathbf{p}}) n_F(\epsilon_{h,\mathbf{p}})$ and the diagonal matrices $\Upsilon_{\mathbf{q},\mathbf{q}'}^i = \delta_{\mathbf{q},\mathbf{q}'} \left(\frac{1}{\tau_{i,\mathbf{q}}} + i\Omega \right)$ and

$$\mathcal{M}_{\mathbf{p},\mathbf{q}}^t = \delta_{\mathbf{q},\mathbf{p}} \frac{2\pi}{A} g^2 \sum_{\mathbf{k}} \delta(\omega_{\mathbf{k}} + \epsilon_{h,\mathbf{p}-\mathbf{k}} - \epsilon_{t,\mathbf{p}}) (n_B(\omega_{\mathbf{k}}) + 1 - n_F(\epsilon_{h,\mathbf{p}-\mathbf{k}})). \quad (27)$$

We first solve for $\varphi_t(\mathbf{p})$ in terms of $\varphi_x(\mathbf{k}), \varphi_h(\mathbf{p})$:

$$\begin{aligned} \varphi_t(\mathbf{p}) &= \frac{2\pi}{A} g^2 \sum_{\mathbf{k}} (\mathcal{M}^t + \Upsilon_t)_{\mathbf{p},\mathbf{p}}^{-1} \delta(\omega_{\mathbf{k}} + \epsilon_{h,\mathbf{p}-\mathbf{k}} - \epsilon_{t,\mathbf{p}}) \\ &\quad \times \left((n_F(\epsilon_{h,\mathbf{p}-\mathbf{k}}) - n_F(\epsilon_{t,\mathbf{p}})) \varphi_x(\mathbf{k}) + (n_B(\omega_{\mathbf{k}}) + n_F(\epsilon_{t,\mathbf{p}})) \varphi_h(\mathbf{p} - \mathbf{k}) \right), \end{aligned} \quad (28)$$

By substituting Eq. (28) back into Eqs. (26), we find the following expression for φ_x and φ_h :

$$\varphi_h(\mathbf{p}) = - \left[\mathcal{M}^h + \Upsilon^h - \mathcal{N}^h (\mathcal{M}^x + \Upsilon^x)^{-1} \mathcal{N}^x \right]_{\mathbf{p},\mathbf{q}}^{-1} \mathcal{K}_{\mathbf{q}}^h, \quad (29)$$

$$\varphi_x(\mathbf{k}) = \left[\mathcal{M}^x + \Upsilon^x - \mathcal{N}^x (\mathcal{M}^h + \Upsilon^h)^{-1} \mathcal{N}^h \right]_{\mathbf{k},\mathbf{q}}^{-1} \left(\mathcal{N}_x (\mathcal{M}_h + \Upsilon_h)^{-1} \mathcal{K}^h \right)_{\mathbf{q}}, \quad (30)$$

where repeated indices imply implicit summation, and for brevity we defined the following matrices:

$$\mathcal{M}_{\mathbf{k},\mathbf{q}}^x = \delta_{\mathbf{k},\mathbf{q}} \frac{2\pi}{A} g^2 \sum_{\mathbf{p}} \delta(\omega_{\mathbf{k}} - \epsilon_{t,\mathbf{p}+\mathbf{k}} + \epsilon_{h,\mathbf{p}}) (n_F(\epsilon_{h,\mathbf{p}}) - n_F(\epsilon_{t,\mathbf{k}+\mathbf{p}})) - \frac{4\pi^2}{A^2} g^4 \sum_{\mathbf{p}} \delta(\omega_{\mathbf{k}} - \epsilon_{t,\mathbf{p}+\mathbf{k}} + \epsilon_{h,\mathbf{p}}) \mathcal{Q}_{\mathbf{q},\mathbf{p},\mathbf{k}}^x, \quad (31a)$$

$$\mathcal{N}_{\mathbf{k},\mathbf{q}}^x = \frac{2\pi}{A} g^2 \delta(\omega_{\mathbf{k}} - \epsilon_{t,\mathbf{q}+\mathbf{k}} + \epsilon_{h,\mathbf{q}}) (n_F(\epsilon_{t,\mathbf{q}+\mathbf{k}}) + n_B(\omega_{\mathbf{k}})) - \frac{4\pi^2}{A^2} g^4 \sum_{\mathbf{p}} \delta(\omega_{\mathbf{k}} - \epsilon_{t,\mathbf{p}+\mathbf{k}} + \epsilon_{h,\mathbf{p}}) \mathcal{Q}_{\mathbf{q},\mathbf{p},\mathbf{k}}^h, \quad (31b)$$

$$\mathcal{M}_{\mathbf{p},\mathbf{q}}^h = \delta_{\mathbf{p},\mathbf{q}} \frac{2\pi}{A} g^2 \sum_{\mathbf{k}} \delta(\omega_{\mathbf{k}} + \epsilon_{h,\mathbf{p}} - \epsilon_{t,\mathbf{p}+\mathbf{k}}) (n_F(\epsilon_{t,\mathbf{p}+\mathbf{k}}) + n_B(\omega_{\mathbf{k}})) - \frac{4\pi^2}{A^2} g^4 \sum_{\mathbf{k}} \delta(\omega_{\mathbf{k}} + \epsilon_{h,\mathbf{p}} - \epsilon_{t,\mathbf{p}+\mathbf{k}}) \mathcal{Q}_{\mathbf{q},\mathbf{p},\mathbf{k}}^h, \quad (31c)$$

$$\mathcal{N}_{\mathbf{p},\mathbf{q}}^h = \frac{2\pi}{A} g^2 \delta(\omega_{\mathbf{q}} + \epsilon_{h,\mathbf{p}} - \epsilon_{t,\mathbf{p}+\mathbf{q}}) (n_F(\epsilon_{h,\mathbf{p}}) - n_F(\epsilon_{t,\mathbf{p}+\mathbf{q}})) - \frac{4\pi^2}{A^2} g^4 \sum_{\mathbf{k}} \delta(\omega_{\mathbf{k}} - \epsilon_{t,\mathbf{p}+\mathbf{k}} + \epsilon_{h,\mathbf{p}}) \mathcal{Q}_{\mathbf{q},\mathbf{p},\mathbf{k}}^x, \quad (31d)$$

$$\mathcal{Q}_{\mathbf{q},\mathbf{p},\mathbf{k}}^x = (\Upsilon^t + \mathcal{M}^t)_{\mathbf{p}+\mathbf{k},\mathbf{p}+\mathbf{k}}^{-1} (1 + n_B(\omega_{\mathbf{k}}) - n_F(\epsilon_{h,\mathbf{p}})) \delta(\omega_{\mathbf{q}} + \epsilon_{h,\mathbf{p}+\mathbf{k}-\mathbf{q}} - \epsilon_{t,\mathbf{p}+\mathbf{k}}) (n_F(\epsilon_{h,\mathbf{p}+\mathbf{k}-\mathbf{q}}) - n_F(\epsilon_{t,\mathbf{p}+\mathbf{k}})), \quad (32a)$$

$$\mathcal{Q}_{\mathbf{q},\mathbf{p},\mathbf{k}}^h = (\Upsilon^t + \mathcal{M}^t)_{\mathbf{p}+\mathbf{k},\mathbf{p}+\mathbf{k}}^{-1} (1 + n_B(\omega_{\mathbf{k}}) - n_F(\epsilon_{h,\mathbf{p}})) \delta(\omega_{\mathbf{k}+\mathbf{p}-\mathbf{q}} + \epsilon_{h,\mathbf{q}} - \epsilon_{t,\mathbf{p}+\mathbf{k}}) (n_B(\omega_{\mathbf{k}+\mathbf{p}-\mathbf{q}}) + n_F(\epsilon_{t,\mathbf{p}+\mathbf{k}})). \quad (32b)$$

In Eqs. (31) we keep corrections which, although for-

mally of order $O(g^4)$, may become relevant close to res-

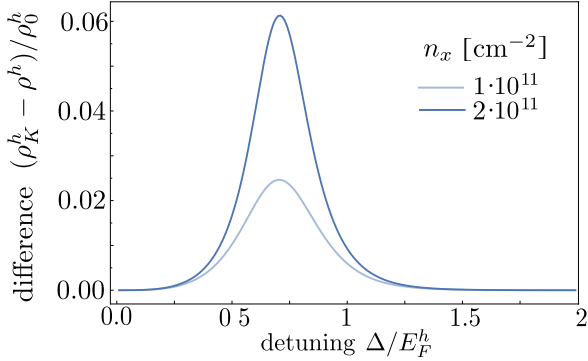


FIG. 6. **Comparison of Kubo and Boltzmann approaches for the hole resistivity.** Difference of the hole resistivities as a function of the detuning Δ as obtained from Kubo's formula to leading order, ρ_K^h , and Boltzmann's equations as described in the previous appendix, ρ^h , for $t = 1$ meV, $T = 5.8$ K and for different values of the exciton density n_x . The relative difference arising from the $\mathcal{O}(g^4)$ corrections included in the kinetic theory treatment, is of a few percent of the background resistivity ρ_0^h .

onance – see discussion in the next section.

We then obtain the conductivities Eq. (25) by a numerical evaluation of Eqs. (28)–(30) and their building blocks Eqs. (31), (32), with the choice $\tau_{i,\mathbf{q}} = \tau_0$ for all $i \in \{h, x, t\}$.

Linear response from Kubo's formula

Since the system hosts a small parameter, we can also analyze the conductivity by evaluating Kubo's formula

$$\sigma_{ab}^h(\mathbf{q}, \omega) = \frac{ie^2}{\omega} \left[\chi_{\mathbf{j}_a \mathbf{j}_b}^R(\mathbf{q}, \omega) + \delta_{ab} \frac{\langle n_h \rangle}{m_h} \right], \quad (33)$$

where $\chi_{\mathbf{j}_a \mathbf{j}_b}^R(\mathbf{q}, \omega)$ is the retarded current-current response function, n_h is the hole density, and $a, b \in \{x, y\}$. To lowest order in g , the diagrammatic expression for $\chi_{\mathbf{j}_a \mathbf{j}_b}^R(\mathbf{q}, \omega)$

see Eq. (35). By combining Eq. (33) and Eq. (37), we can express the conductivity in a standard form

$$\sigma_{xx}^h(\omega = 0) \frac{h}{e^2} = \int_{-\mu}^{\infty} d\xi (\xi + \mu) n'_F(\xi) \tau_{\text{tot}}(\xi), \quad (40)$$

where $\tau_{\text{tot}}^{-1}(\xi) = -2\text{Im}\Sigma_b^R(k(\xi + \mu), \xi)$.

The linear response result Eq. (40) coincides with that obtained by the kinetic method in the previous subsection, to the leading order $\mathcal{O}(g^2)$. Indeed, the term of

yields

$$\chi_{\mathbf{j}_a \mathbf{j}_b}^R(\mathbf{q}, \omega) = \text{---} \bullet \text{---} + \mathcal{O}(g^4), \quad (34)$$

where the thick blue lines denote hole propagators, which are obtained by solving Dyson's equation to order $\mathcal{O}(g^2)$:

$$\longrightarrow = \longrightarrow + \longrightarrow \text{ (35)}$$

In Eq. (35), light-blue, red and squiggly lines denote bare-hole, trion and exciton propagators:

$$\begin{aligned}
 \xrightarrow{\quad} &= \frac{1}{\omega - \xi^h(\mathbf{p}) + i/2\tau_{h,\mathbf{q}}^0} \\
 \xrightarrow{\quad} &= \frac{1}{\omega - \xi^t(\mathbf{p}) + i/2\tau_{t,\mathbf{q}}^0} \\
 \sim \xrightarrow{\quad} &= \frac{1}{\omega - \omega(\mathbf{k}) + i/2\tau_{x,\mathbf{q}}^0},
 \end{aligned} \tag{36}$$

where we have modelled background scattering by adding a finite line broadening $1/2\tau_{i,\mathbf{q}} = 1/2\tau_0$. Evaluating these diagrams and neglecting vertex corrections, one obtains the standard result

$$\begin{aligned} & \lim_{\omega \rightarrow 0} \frac{1}{\omega} \left(\chi_{\mathbf{j}_x \mathbf{j}_x}^R(0, \omega) + \frac{\langle n_h \rangle}{m_h} \right) \\ &= \frac{i}{4\pi} \int_0^\infty dE E \int \frac{dz}{2\pi} \frac{\mathcal{A}(k(E), z)}{\text{Im} \Sigma_h^R(k(E), z)} n_F'(z), \end{aligned} \quad (37)$$

where $k(E)^2 = 2m_h E$. The current-current response function can be expressed directly in terms of the hole spectral function

$$\mathcal{A}(\mathbf{k}, z) = -2\text{Im}G^R(\mathbf{k}, z) \quad (38)$$

and their perturbatively evaluated self energy

$$\Sigma_h^R(\mathbf{k}, \omega) = -g^2 \int \frac{d^2 \mathbf{q}}{(2\pi)^2} \frac{n_F(\epsilon_{t, \mathbf{q} + \mathbf{k}}) + n_B(\omega_{\mathbf{q}})}{\epsilon_{t, \mathbf{q} + \mathbf{k}} - i/2\tau_{t, \mathbf{q} + \mathbf{k}} - \omega - \omega_{\mathbf{q}} - i/2\tau_x(\mathbf{q})} - \frac{i}{2\tau_h(\mathbf{k})} + \mathcal{O}(g^4); \quad (39)$$

order g^2 in \mathcal{M}^h in Eq. (31c), responsible for the most relevant many-body contribution to the hole resistivity, is identical to $2\text{Im}\Sigma_h^R(\mathbf{p}, \epsilon_{\mathbf{p},h})$ in Eq. (39) in the limit $1/2\tau_{i,\mathbf{q}} \rightarrow 0^+$. The Boltzmann approach also takes into account higher orders in g^2 , however we checked numerically that $\mathcal{O}(g^4)$ corrections to the hole resistivity, albeit finite, are small for the considered parameters, see Fig. 6.

On the kinetic theory side, such formally $\mathcal{O}(g^4)$ corrections arise from the rightmost terms in Eqs. (31), and

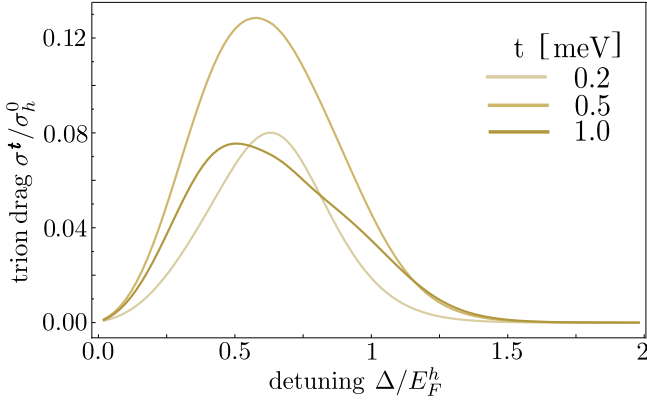


FIG. 7. **Trion drag across resonance.** Trion conductivity as a function of the detuning Δ , for $T = 5.8$ K and different values of the tunneling parameter t .

especially in the hole resistivity case from $Q(\mathbf{p}, \mathbf{q}) \equiv -\frac{4\pi^2}{A^2} g^4 \sum_{\mathbf{k}} \delta(\omega_{\mathbf{k}} + \epsilon_{h, \mathbf{p}} - \epsilon_{t, \mathbf{p} + \mathbf{k}}) Q_{\mathbf{q}, \mathbf{p}, \mathbf{k}}^h$ in Eq. (31c). This correction becomes relevant for $\mathbf{p} \approx \mathbf{q}$ at small temperatures $k_B T \ll \hbar^2 n_x / m_x$, where the population of excitons at small momenta $\mathbf{k} \approx \mathbf{0}$ is a sizeable fraction of n_x . In this regime, for small values of disorder, it can be that $\Upsilon^t + \mathcal{M}^t$ is dominated by $\mathcal{M}^t \propto g^2 n_x$. This in turn implies that $Q(\mathbf{q}, \mathbf{q}) \sim g^2 n_x$, in contrast to its formal magnitude $\mathcal{O}(g^4)$. This provides a relevant contribution to the hole resistivity obtained from the kinetic theory method, which in the formalism of Kubo's equation would correspond to higher-order diagrammatic corrections to the bare conductivity bubble calculated in Eq. (37).

Trions

The trions exhibit a drag effect similarly to the excitons. The resulting rion conductivity depends strongly on resonant interactions, see Fig. 7. For small values of the interaction parameter $g \propto t$ and small temperature, σ^t reaches a maximum in the vicinity of the resonance ($\Delta \approx \Delta_*$) and increases with increasing g , as expected

from the general discussion of hole-exciton-trion scattering given in the main text. At larger g , where $\mathcal{M}_i \gtrsim \Upsilon_i$ for $i \in \{h, x, t\}$, many-body corrections to the relaxation times become important. As a result, with increasing g , σ^h decreases, σ^x saturates, and σ^t decreases before it saturates. Such corrections at large g also entail less evident signatures nearby resonance, especially noticeable in the trion case. Remarkably, we find that the trion conductivity takes values of the same order of magnitude as the exciton conductivity. Therefore, the individual conductivities can be resolved by separately measuring charge currents in both the middle and the lower layer.

Hydrodynamic model for ac conductivities

The three-fluid model of the main text can be solved analytically. The ac conductivities of the three particle species are obtained as:

$$\sigma^i(\Omega) = \frac{A_i}{1/\tau_i + i\Omega + B_i} \frac{n_i}{n_h} \sigma^h(\Omega), \quad (41)$$

$$\sigma^h(\Omega) = \frac{e^2 n_h / m_h}{1/\tau_h + i\Omega + \sum_{i=x,t} C_i (1 - \frac{A_i}{i\Omega + 1/\tau_i + B_i})}, \quad (42)$$

where we defined

$$A_i = \alpha_{ih} \frac{n_h}{m_i} + \frac{\alpha_{ih} \alpha_{tx} n_{\bar{i}} n_h / m_i}{\alpha_{ih} n_h + \alpha_{tx} n_i + i\Omega + 1/\tau_{\bar{i}}}, \quad (43a)$$

$$B_i = \frac{\alpha_{tx} n_{\bar{i}}}{m_i} + \frac{\alpha_{ih} n_h}{m_i} - \frac{\alpha_{tx}^2 n_x n_t / m_i}{\alpha_{ih} n_h + \alpha_{tx} n_i + i\Omega + 1/\tau_{\bar{i}}}, \quad (43b)$$

$$C_i = \alpha_{ih} n_i / m_h \quad (43c)$$

and use the shorthand notation $i = x, t \leftrightarrow \bar{i} = t, x$ respectively.

We use Eqs. (41), (42) to fit the ac conductivities, obtained by solving the system of coupled Boltzmann's equations as described in the first appendix, reported in the main text. We find the following values for the fitting parameters: $\tau_h = 9.4$ ps, $\tau_x = 10.0$ ps, $\tau_t = 2.9$ ps, $\alpha_{th} = 0.64 \frac{m_0}{n_0 \tau_0}$, $\alpha_{xh} = -0.48 \frac{m_0}{n_0 \tau_0}$, $\alpha_{tx} = 0.50 \frac{m_0}{n_0 \tau_0}$, where $n_0 = 10^{12} \text{ cm}^{-2}$, $m_0 = 0.25 m_e$, and $\tau_0 = 10$ ps.